

IEEE Copyright Notice

© 2020 IEEE. Personal use of this material is permitted. Permission from IEEE must be obtained for all other uses, in any current or future media, including reprinting/republishing this material for advertising or promotional purposes, creating new collective works, for resale or redistribution to servers or lists, or reuse of any copyrighted component of this work in other works.

Submitted to: IEEE Transactions on Neural Networks and Learning Systems
on 12/25/2020

Manuscript ID: **TNNLS-2020-P-16074**

Toward Real-World BCI: CCSPNet, A Compact Subject-Independent Motor Imagery Framework

Mahbod Nouri^{ID}, Faraz Moradi^{ID}, Hafez Ghaemi^{ID}, and Ali Motie Nasrabadi^{ID}

Abstract— A conventional brain-computer interface (BCI) requires a complete data gathering, training, and calibration phase for each user before it can be used. This preliminary phase is time-consuming and should be done under the supervision of technical experts commonly in laboratories for the BCI to function properly. In recent years, a number of subject-independent (SI) BCIs have been developed. However, there are many problems preventing them from being used in real-world BCI applications. A lower accuracy than the subject-dependent (SD) approach and a relatively high run-time of models with a large number of model parameters are the most important ones. Therefore, a real-world BCI application would greatly benefit from a compact subject-independent BCI framework, ready to use immediately after the user puts it on, and suitable for low-power edge-computing and applications in the emerging area of internet of things (IoT). We propose a novel subject-independent BCI framework named CCSPNet (Convolutional Common Spatial Pattern Network) that is trained on the motor imagery (MI) paradigm of a large-scale electroencephalography (EEG) signals database consisting of 400 trials for every 54 subjects performing two-class hand-movement MI tasks. The proposed framework applies a wavelet kernel convolutional neural network (WKCNN) and a temporal convolutional neural network (TCNN) in order to represent and extract the diverse frequency behavior and spectral patterns of EEG signals. The convolutional layers' outputs go through a common spatial pattern (CSP) algorithm for class discrimination and spatial feature extraction. The number of CSP features is reduced by a dense neural network, and the final class label is determined by a linear discriminative analysis (LDA). The final SD and SI classification accuracies of the proposed framework match the best results obtained on the largest motor-imagery dataset present in the BCI literature, with 99.993 percent fewer model parameters.

Index Terms— Brain-computer interface (BCI), motor imagery (MI), subject-independent, electroencephalography (EEG), convolutional neural network (CNN), wavelet transform, deep learning (DL), common spatial pattern (CSP)

I. INTRODUCTION

BRAIN-COMPUTER interface (BCI) is a type of human-computer interaction that exploits several different methods to decode, interpret, and classify human intentions,

decisions, and neural activities in order to create a communication pathway between the brain and external devices [1]-[2]. One of the most prevalent types of BCI uses recorded brain signals, known as electroencephalography (EEG). These signals are recorded by installing a special cap, known as EEG cap, on the subject's head. This cap has a specific number of electrodes, also known as channels, that record the subject's brain signals from different areas of the brain [3]. There are generally three different paradigms in the BCI domain [24]. These paradigms include motor imagery (MI) [4]-[5], event-related potential (ERP) [6]-[7], and steady-state visually evoked potential (SSVEP) [8].

Motor imagery, which is the main focus of this paper, can be defined as a mental process in which a person imagines performing a particular action without any physical movement [9]-[10]. Motor imagery could have many potential real-world applications, especially for powering equipment designed to help disabled people execute specific actions they could not have performed otherwise due to their disability [11]-[12]. However, there are three significant challenges to overcome in creating a general-purpose subject-independent motor imagery brain-computer interface. First of all, most of the research in the MI domain is subject-dependent; i.e., the proposed models require data recording, training and calibration for individual subjects. This preliminary phase and the need for possibly different hyperparameters to adapt to a new subject would render the implementation of a general-purpose BCI, especially a commercial product, impossible. Secondly, any subject-independent model developed for real-world and commercial applications, e.g., portable wearable devices or smart wheelchairs designed for disabled people [13]-[14], must be computationally efficient with a small amount of memory required. If these devices had too much computational power and memory capacity, they would not be affordable by the general public. A compact framework with few parameters and a relatively short run-time (on a device having inexpensive hardware) could address this challenge. It is worthwhile to mention that with the recent advances in the area of Internet of Things (IoT) and edge-computing [15]-[16], this challenge may become even more paramount in the coming years as the need

Submitted on 12/25/2020.

Mahbod Nouri is a research assistant at the Advanced Robotics and Intelligent Systems Lab, School of Electrical and Computer Engineering, and a mechanical engineering Alumnus of University of Tehran, Iran (e-mail: ma.nouri@ut.ac.ir).

Faraz Moradi is a BCI researcher, and a biomedical engineering alumnus of the Islamic Azad University, Science and Research Branch, Tehran, Iran (e-mail: moradi.faraz1998@gmail.com).

Hafez Ghaemi is a graduate student at the Department of Control and Computer Engineering, Polytechnic University of Turin, Italy (e-mail: hafez.ghaemi@studenti.polito.it).

Ali M. Nasrabadi is a full professor at Shahed University, and a scientific advisor at the National Brain Mapping Laboratory, Tehran, Iran (e-mail: nasrabadi@shahed.ac.ir).

for optimized and fast computation in distributed low-power edge-computing-based applications will be much more significant than conventional or cloud applications [16]-[17]. In a real-world BCI application, the EEG signals can be recorded with mobile headwear such as [18]-[19], and the device can utilize distributed edge-computing to predict the subject's decision in real-time [20]. Lastly, any model which is going to be used in real-world applications must have acceptable accuracy. We consider an appropriate lower limit for the average test accuracy of a subject-independent BCI model to be equal or higher than the average subject-dependent (SD) accuracy of the same model.

Numerous models have been proposed to address one or two of the aforementioned problems. Our main contribution is developing a framework satisfying all these three conditions (compactness, subject-independence, and accuracy) on a large-scale motor imagery dataset [21].

The remainder of this article is organized as follows:

In section II, we will mention and discuss some of the methods and efforts addressing the above challenges. Section III will be dedicated to describing the dataset used in our work. In section IV, the proposed framework and architecture will be described. The classification results of our framework are presented in section V. An analysis of our results and a comparison with the other methods is conducted in section VI. A brief conclusion is offered in section VII.

II. RELATED WORKS

The majority of research papers in the BCI literature are concerned with the subject-dependent approach. As mentioned before, all SD models require a training and calibration phase to adapt to each subject's brain patterns. Many of these SD models have used conventional source analysis [22]-[23] or machine learning (ML) algorithms for classification. Wang *et al.* [24] used common spatial patterns (CSP) for channel selection and linear discriminant analysis (LDA) for classification. Dong *et al.* [25] proposed a hierarchical method for extending Support Vector Machine (SVM) to be used on a 4-class BCI dataset. They used one-versus-rest CSP and one-versus-one CSP in each of their SVM layers. Recently, the utilization of deep learning (DL) algorithms for decoding EEG signals and task classification has become a trend in the BCI literature. Lawhern *et al.* have proposed a well-known compact convolutional neural network (CNN), known as EEGNet [26], that is widely applied on various datasets and all BCI paradigms for task classification, and, in many cases, yields an acceptable subject-dependent accuracy. There are models inspired by EEGNet, which are also compact and suitable for low-power edge-computing [27]-[29]. EEGNet was also applied to the dataset used in this research. The results are presented and discussed in sections V and VI. Zhang *et al.* have also taken a deep learning approach, and applied complex Morlet wavelet transform [30] on the EEG data to feed their relatively compact convolutional neural network with a time-frequency tensor [31]. Other time-frequency analysis methods, such as short-time Fourier transform (STFT), have been utilized to create a more suitable input for convolutional neural networks [32]-[33]. One of the main challenges facing DL-BCI researchers is the lack of large-scale datasets (both in the number of subjects

and trials per subject) to be utilized in deep learning algorithms. A possible solution to this problem is data augmentation. Traditional data augmentation approaches like empirical mode decomposition [31], [34] and geometric transforms such as rotation, flipping, and zooming [32] have been used on EEG signals. Novel approaches such as data augmentation using generative adversarial networks (GANs [35]) have also been implemented to achieve higher accuracies with DL models for SD motor imagery classification [36]-[37].

There are also approaches lying in the middle of the SD/SI spectrum. These methods are usually used to reduce the calibration time (mostly by reducing data recording and model training time) required in subject-dependent BCI. For example, in transfer learning, available data from other subjects is used to fine-tune the model before training on new subjects [38], [39], [40].

The pure subject-independent approach is much less prevalent than the subject-dependent approach in the realm of BCI. Although usually yielding a lower average accuracy than the SD approach, non-DL machine learning algorithms have been tried for subject-independent BCI [41]-[42]. This low SI accuracy may be attributed to the fact that spectral-spatial patterns of different subjects' brain signals vary significantly, and traditional ML algorithms have a limited capacity for complex pattern recognition [43]. Deep learning and neural networks have the unique ability to adapt to highly variable data and detect complex patterns and therefore, can be effectively used in the SI BCI approach. However, the use of deep learning in subject-independent BCI is rare. One of the first works that have taken advantage of a large-scale MI database (also used in this work and recorded by Lee *et al.* [21]) to implement a DL framework for motor imagery paradigm have used a convolutional neural network with about 72 million parameters [44]. In this framework, the parallel CNNs take CSP features extracted from frequency bins, selected based on an information-theoretic analysis, as input. A concatenation fusion layer and a fully connected layer are used at the end to output the predicted class labels.

III. DATASET

The dataset used to evaluate the performance of the proposed framework (CCSPNet) is an open-source BCI database recorded by Lee *et al.* [21]. This dataset can be accessed through [45]. It is one of the largest BCI datasets recorded to this date. 54 healthy subjects, including 25 females and 29 males, aged 24 to 35, went through the same experiment in two sessions, among whom were 16 experienced BCI users and 34 inexperienced ones. The subjects were seated in comfortable chairs and were asked to relax their muscles. 62 Ag/AgCl electrodes were used to capture EEG signals with a sampling rate of 1000 Hz. Furthermore, four electrodes recorded EMG signals, which are stored in the database as "EEG_Artifact" for each individual. The channel configuration is presented in Fig 1. The reference electrode (Cz) is indicated by black. The experiment consists of the three BCI paradigms (SSVEP, ERP, and MI) conducted in two similar sessions, in two different days. Each session is composed of a training and a testing phase, each including 100 trials. Our focus is on the motor imagery paradigm task classification. During each

training trial of the MI paradigm, subjects were prompted to execute a 2-class motor imagery task. The timing of a single MI trial in the training phase is illustrated in Fig 2. At the beginning of the training trial, as preparation, a black fixation cross appeared on the screen center for 3 seconds. Afterward, a prompt instructing the subjects to perform the MI task was shown. The prompt was a left or right arrow standing for the movement imagination of left or right hand. After each trial, a period of 6 s (± 1.5) blank screen was shown, indicating the rest period.

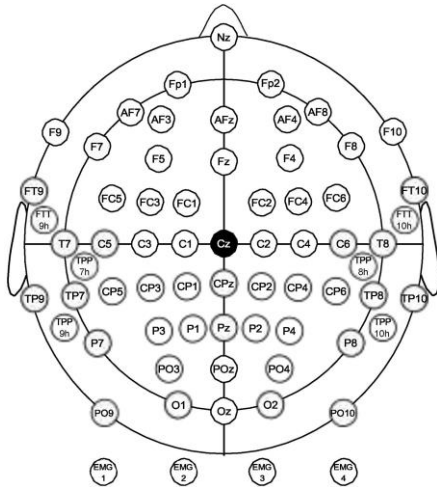


Fig 1. (Image adopted from [21] which is under the terms of the Creative Commons Attribution License) The 62 EEG and 4 EMG electrodes configuration. The EEG electrodes are placed according to the 10-20 international system. The reference electrode (Cz) is indicated by black.

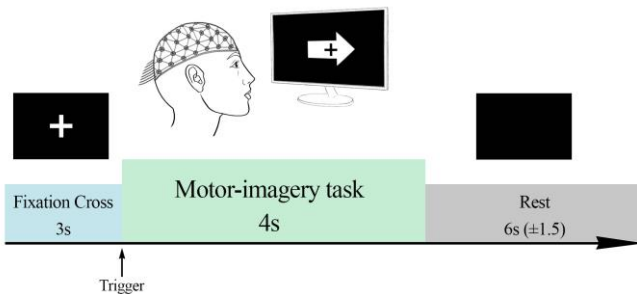


Fig 2. The binary class MI paradigm EEG signal recoding

When the training phase ended, a set of online classifiers based on Common Spatial Pattern (CSP) and Linear Discriminant Analysis (LDA) was trained using the recorded EEG signals. In the testing phase, subjects perform the MI tasks, and their performance is evaluated. Real-time neurofeedback in the shape of a right or left arrow appeared on the screen, denoting the predicted class. This feedback can be effective in improving the user's performance in future test trials. After obtaining the accuracies of the test phase for each subject and paradigm, Lee *et al.* [21] have defined the BCI illiteracy threshold as 70% accuracy. Interestingly, the MI paradigm showed the lowest average, the most variation of accuracy among subjects, and the maximum number of BCI illiterate users compared to other paradigms. The results of this online classifier in the MI paradigm are presented and compared to our proposed method's in sections V and VI.

IV. METHOD

The architecture proposed, which is named CCSPNet (Convolutional Common Spatial Pattern Network), exploits the benefits of signal processing and time-frequency analysis, traditional machine learning approaches, and novel deep learning algorithms to implement a compact framework that can be used in both SI and SD motor imagery and achieve high classification accuracies. The most important advantages of the proposed method compared to other deep-learning motor imagery BCI frameworks is its lower training and run time, fewer parameters, which makes it a good candidate for real-time MI-BCI applications related to low-power edge-computing and IoT.

In the following paragraphs, the model architecture and classification procedure will be described.

The raw EEG data for a single trial is denoted by a matrix $x \in \mathbb{R}^{C \times T}$ where C is the number of channels (electrodes), and T is defined as the number of sample points. In this dataset, $C = 62$ and $T = 4000$ for the raw EEG signal. Since the dataset is large, for the purpose of better computation efficiency and code vectorization, all training trials have been concatenated into a 3-D matrix of dimensions $(N, 62, 4000)$ designated as X . Similarly, *Label* vector is constructed by concatenating all trial labels into a one-dimensional vector of size N .

A. Preprocessing

First, the EEG signals were trimmed, and the timepoints between 1000 to 3500 milliseconds were extracted. Motor imagery tasks are generally associated with the μ (7.5 – 12.5 Hz) and β (12.5 – 30 Hz) EEG frequency bands. This association is related to the Event-Related Desynchronization and Event-Related Synchronization (ERD/ERS) phenomena. [46]-[33]. Consequently, we are mostly interested in the frequency ranges below 40 Hz. Based on the Nyquist theory [47], the signals were down-sampled to 100 Hz to ensure that the information from the desired frequency ranges is extracted. EEG signals related to motor imagery tasks are mostly generated in the motor cortex [48] (electrodes in the central region of Fig. 1). However, the EEG signals do not have a perfect spatial resolution, i.e., the electrodes may capture information from areas of the brain other than those in their vicinity. Therefore, signals from electrodes not highlighted in Fig. 1 might also contain useful information related to MI tasks. Many works have removed electrodes other than those traditionally associated with their relative BCI paradigm, in this case, motor imagery [44]-[31]. Furthermore, many algorithms have been proposed for efficient EEG channel selection [49]-[50]. The reason behind this may be to build a more compact model or to reduce the training time. Others have included all channels when feeding their model [51]-[52]. Because the proposed architecture (CCSPNet) is compact enough and requires all the relevant information, no channel reduction is performed.

A fifth-order band-pass Butterworth filter with the conventional frequency band [8, 30 Hz] was applied to the EEG signals. This filter frequency band is represented by f . The

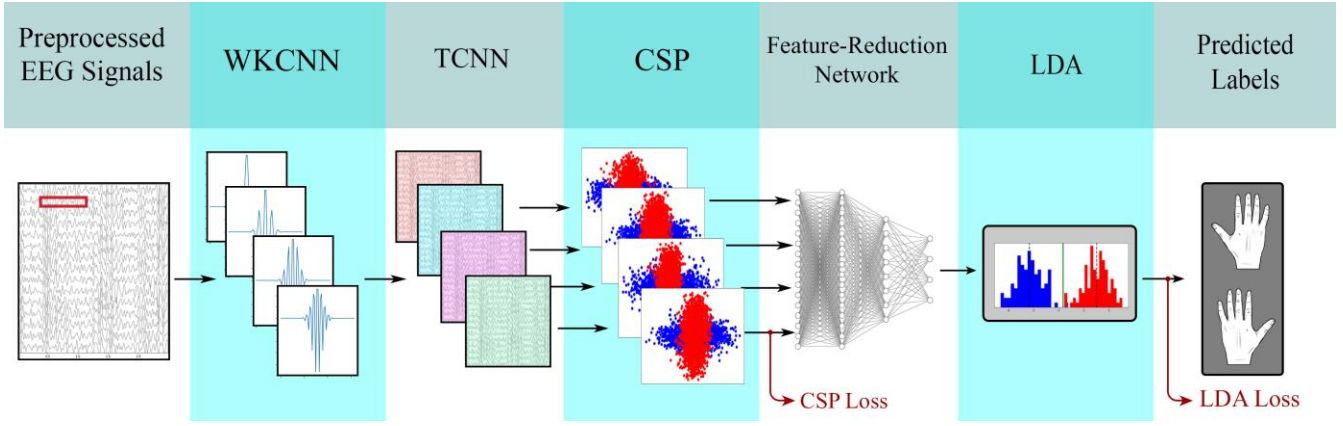


Fig 3. Graphical representation of the proposed subject-independent motor imagery framework (CCSPNet); The framework starts with a wavelet kernel convolutional neural network acting upon the preprocessed EEG signals with one-dimensional wavelet kernels (first and second columns). Afterwards, a temporal convolutional neural network with normal one-dimensional convolutional kernels will be applied to the data (third column). These two networks filter the signals spectrally (with respect to time and frequency). Then, the CSP module filters the signals spatially (with respect to channels), and extracts spatial features from them (Fourth column). At this step the first loss function (CSP loss) is calculated. A feature-reduction dense neural network reduces the high-dimensional CSP outputs to improve the classification performance of the LDA module (fifth column). Finally, the LDA module calculates the second loss function (LDA loss) and outputs the class labels (sixth and seventh column). Detailed architecture of the CCSPNet framework is presented in Table I.

TABLE I. Detailed Architecture for the CCSPNet framework

Module	Layer	Kernel Size	Output Dimension	Activation	Mode
-	Input		(N, 1, 64, 250)		
Wavelet-Kernel CNN	Convolution	32×1	(N, 4, 64, 250)		same
Temporal CNN	Convolution	64×1	(N, 4, 64, 250)		same
Trainable CSP			(N, 4, 4, 2)		
Feature Reduction Network	Flatten		(N, 32)		
	Batch Norm 1D		(N, 4, 4, 2)		
	Dense		(N, 16)	Sigmoid	
	Batch Norm 1D		(N, 16)		
	Dense		(N, 8)	Sigmoid	
	Batch Norm 1D		(N, 8)		
Trainable LDA (Classifier)	Dense		(N, 4)		
			(N, 1)		

filtering operation is denoted by \odot . The matrix X will be filtered as follows:

$$X = f \odot X \quad (1)$$

All preprocessing steps are performed in *MATLAB ver. R2019b*.

B. The Proposed Method

The graphical representation of the CCSPNet framework is depicted in Fig. 3. The framework's layer information and detailed architecture are given in Table I. The calcification process consists of five main steps. These steps include 1- A wavelet kernel convolutional neural network (WKCNN) for smooth filtering 2- A temporal convolutional neural network (TCNN) to learn frequency filters and data augmentation, 3- Common Spatial Pattern (CSP) algorithm performed on the CNN outputs, 4- Feature-reduction dense artificial neural network, 5- Linear Discriminant Analysis (LDA) to classify the reduced features.

The main structural hyperparameters associated with the model include the number of wavelet filters ($wn = 4$), the kernel length of wavelet filters ($wkl = 64$), the number of temporal convolutions in the TCNN ($F = 4$) and their kernel

length ($kl = 32$), half the number of eigenvectors to be extracted from CSP ($m = 2$), and the number of neurons in the feature-reduction network ($nn = [16, 8, 4]$).

The network input is the preprocessed data ($X \in \mathbb{R}^{N_{trials} \times 62 \times 250}$, $Label \in \mathbb{R}^{N_{trials}}$) divided into batches ($batchSize = b$). For the sake of explanation, we assume that the first batch is being fed into the model:

$$X_{input} = X[1:b] \quad (2)$$

$$Label_{input} = Label[1:b] \quad (3)$$

1. Kernel Wavelet Convolutional Neural Network (WKCNN)

As the first step of the training procedure, a one-layer convolutional neural network with one-dimensional kernels will be applied to the data. However, instead of normal convolutional kernels, wavelets are used to perform the time-domain convolutions. This specific CNN architecture is proposed by Li *et al.* [53]. The wavelet minimum and maximum frequencies (8 and 30 Hz) are consistent with the Butterworth filter range used during the preprocessing. There are three trainable parameters associated with the WKCNN, which are

Algorithm 1. The CCSPNet framework classification algorithm

Input: a set of training samples

- **b**: Batch size
- $\mathbf{x} \in \mathbb{R}^{C \times T}$: EEG data from a single trial with C channels, and T timepoints
- $\mathbf{X} = \{\mathbf{x}_i\}_{i=1}^b$: A set containing b individual EEG trials
- $\mathbf{label}_{\text{actual}} \in \{0, 1\}$: The actual class label of a single trial
- $\mathbf{Label}_{\text{actual}} = \{\mathbf{label}_i\}_{i=1}^b$: A set containing b trials' class labels corresponding to \mathbf{X}
- f : Fifth-order [8, 30 Hz] Butterworth filter
- wn : The number of wavelet filters. In the framework $wn = 4$
- F : the number of temporal convolutions (filters). In the framework $F = 4$
- m : The number of eigenvectors to be extracted from CSP projection matrices for each class. In the framework $m = 2$.
- nn : The number of neurons in the dense neural network's last layer (the number of LDA's inputs)

Output: Predicted labels

- $\mathbf{label}_{\text{pred}} \in \{0, 1\}$: The predicted class label of a single trial
- $\mathbf{Label}_{\text{pred}} = \{\mathbf{label}_i\}_{i=1}^b$: A set containing trials' predicted class labels corresponding to the input \mathbf{X}

Operators:

- \odot : The fifth-order Butterworth band-pass filter operator
- $WKCNN$: The wavelet kernel convolutional neural network operator.
- $TCNN$: The temporal convolutional neural network operator.
- $GEP(\mathbf{X}, \mathbf{Label})$: Operator that solves the generalized eigen value problem and returns a projection matrix \mathbf{W}
- FRN : The feature-reduction network's operator
- LDA : Linear discriminant analysis classifier which returns the predicted class label

Procedure:

$\mathbf{X} = f \odot \mathbf{X}$

$\mathbf{X}_w = WKCNN(\mathbf{X})$

$\mathbf{X}_w = \{\mathbf{X}_{w_i}\}_{i=1}^{wn}$

$\mathbf{X}_F = TCNN(\mathbf{X}_w)$

$\mathbf{X}_F = \{\mathbf{X}_{F_i}\}_{i=1}^F$

CSP

for $i = 1$ **to** F :

$\mathbf{W}_i = GEP(\mathbf{X}_F[i], \mathbf{Label})$

 # shape: (62, 62)

$\mathbf{W}_{ext_i} = \text{concatenate}(\mathbf{W}_i[1:m], \mathbf{W}_i[\text{end} - m, \text{end}])$

 # shape: (62, 2m)

$\mathbf{Y}_i = \mathbf{W}_{ext_i}^T \mathbf{X}_F[i]$

 # shape: (b, 2m, T)

$\mathbf{V}_i = \log(\text{var}(\mathbf{Y}_i))$

 # shape: (b, 2m)

end

$\mathbf{V} = \text{concatenate}\{\mathbf{V}_i\}$

shape: (b, 2m, F)

$\mathbf{input}_{lda} = FRN(\mathbf{V})$

shape: (b, nn)

$\mathbf{Label}_{\text{pred}} = LDA(\mathbf{input}_{lda})$

updated by backpropagation and the optimization algorithm during training. The wavelet frequencies, full width at half maximum, and a gaussian exponent coefficient for adjusting the wavelet magnitude are the trainable parameters. The wavelets consist of the multiplication of a cosine wave and a Gaussian wave:

$$\text{wavelet} = \text{csw} \times \text{gus} \quad (4)$$

$$\text{csw} = \cos(2\pi \times \text{freq} \times \text{timevec}) \quad (5)$$

$$\text{gus} = \exp(-\text{coef} \times \frac{\text{timevec}^2}{f_{whm}^2}) \quad (6)$$

$$\text{timevec} = \frac{wkl}{f_s} \quad (7)$$

Where *coef* is the exponent coefficient for adjusting the wavelet magnitude, *freq* is the wavelet frequency, *timevec* is the time vector by which the wavelet is constructed, *wkl* is the wavelet kernel length, *f_s* is the sampling frequency after down-sampling (100 Hz), and *fwhm* is the Gaussian signal's full width at half maximum. The wavelet frequencies are initialized linearly between 8 and 30 Hz.

The wavelet then will be applied to the input data as a convolution kernel:

$$\mathbf{X}_w = WKCNN(\mathbf{X}_{\text{input}}) \quad (8)$$

The *WKCNN* operator denotes the operation of the wavelet convolutional neural network. X_w has dimensions $(b, 4, 62, 250)$.

2. Temporal Convolutional Neural Network (TCNN)

As illustrated in Fig. 3, the second step of the algorithm is a 2-D convolutional layer (CNN) consisting of four temporal convolutions. In this layer, four dynamic kernels with dimension $(1, k)$ will be applied to the signals. The nomenclature "Temporal Convolution" is used by Lawhern *et al.* [26] to emphasize that this layer acts only upon the signal's timepoints and does not reduce the number of channels. The number of timepoints remains constant by zero-padding after applying the kernel. This method has also been used by Sakhavi *et al.* [54] to extract temporal information from EEG signals. The output of this layer is given below:

$$X_F = TCNN(X_w) \quad (10)$$

The purpose of the first and the second steps (WKCNN and TCNN) is to represent and extract frequency behavior and spectral patterns by learning frequency filters (each represented by a distinct kernel). These filters are able to make the signals better distinguishable by the CSP module. In other words, by dynamically updating both WKCNN and TCNN weights to minimize the cumulative loss function (23) using backpropagation and the Adam optimization algorithm [55], we are able to facilitate the CSP's job to discriminate between MI classes.

X_F has dimensions $(b, 4, 62, 250)$. Now, to better illustrate the third step of the algorithm, we denote X_F as a set with four tensors with shape $(b, 62, 250)$:

$$X_F = \{X_{F_i}^{b \times 62 \times 250}\}_{i=1}^4 \quad (11)$$

3. CSP

A conventional CSP algorithm [24] was performed on each member of X_F . As a result, a set of projection matrices generated by solving four generalized eigenvalue problems is generated as below:

$$X_F, Label_{input} \xrightarrow{\text{solve GEPS}} \{W_i^{62 \times 62}\}_{i=1}^4 \quad (12)$$

Where W_i is X_{F_i} 's corresponding projection matrix and a set of 62 spatial filters that act upon the channels of the data. W_i can be applied to X_{F_i} to filter it spatially. However, to improve the CSP's ability to distinguish between classes, the first and the last m vectors of each W_i are extracted. In the framework, $m = 2$ is chosen. The corresponding $(62, 4)$ matrix consisting of two $(62, 2)$ matrices for representing each class are able to project each trial to its corresponding class's hyperplane. The final set of projection matrices is obtained as below:

$$\{W_{ext_i}\}_{i=1}^F = \{\text{concat}(W_i[1:m], W_i[\text{end} - m, \text{end}])\}_{i=1}^F \quad (13)$$

These projections (each with dimensions $(62, 4)$) were then applied to their corresponding X_{F_i} to generate the CSP outputs Y_i :

$$Y_i = (W_i^T X_{F_i}) \in \mathbb{R}^{b \times 4 \times 250} \quad (14)$$

To extract features from these outputs (spatially filtered signals), the logarithm of the variance of each member of the set $\{Y_i\}_{i=1}^4$ was calculated:

$$\{V_i\}_{i=1}^F = \{\log(\text{var}(Y_i))\}_{i=1}^F \quad (14)$$

Where $V_i \in \mathbb{R}^{b \times 4}$.

In this step, we define the first loss function named CSPLoss. This function uses a target vector with size $2m$ (the first and second m indices are 0 or 1 depending on the actual class label.) to calculate binary cross-entropy between the actual input and the target vectors [56]:

$$CSPLoss(V_i) = BCELoss(\text{input} = V_i, \text{target} = \text{concat}\{[1 - \text{actualLabel}]_2, [\text{actualLabel}]_2\}) \quad (15)$$

Where *BCELoss* measures the unweighted binary cross-entropy between its input (in this case, the CSP features) and the target vector (in this case, a vector with size 4 that has the class label as its last 2 indices and the opposite class label as its first 2 indices.). The unweighted *BCELoss* between X and Y is defined as below:

$$l(X, Y) = L = \{l_1, \dots, l_b\}^T \quad (16)$$

$$l_n = -[y_n \cdot \log x_n + (1 - y_n) \cdot \log(1 - x_n)] \quad (17)$$

Where b is the batch size.

The target vector is the optimal feature vector representing the corresponding class's hyperplane. By minimizing the *BCELoss*, we are trying to minimize the distance between the real CSP feature vector and this optimal vector to enhance the distinguishing ability of the CSP. In addition, using this loss function can prevent overfitting by letting us extract mathematically meaningful features from the CSP instead of any arbitrary feature that would separate the LDA density functions (This happens when the LDALoss function (22) is the only loss function used.).

4. Feature-Reduction Network (FRN)

The final features extracted from CSP for each four CSP outputs were concatenated into a single matrix:

$$V = (\text{concatenate}\{V_i\}_{i=1}^4) \in \mathbb{R}^{b \times 16} \quad (18)$$

The classic LDA algorithm for classifying CSP features does not perform well on high-dimensional data, and several approaches have been proposed to tackle this problem [57]-[58]. We have proposed a novel method for selecting the best possible features for the LDA. In this step, we have utilized a dense artificial neural network (ANN) for feature reduction.

This ANN consists of three dense layers with [16, 8, 4] neurons. The weights will be updated by backpropagation and the optimization algorithm to minimize the LDALoss (22). The FRN's output will be given to the LDA for classification. The FRN operator acts as below:

$$X_L^{b \times 4} = FRN(V) \quad (19)$$

TABLE II. The CCSPNet framework default hyperparameters

Hyperparameter	Value
Batch Size (SI)	1024
Wavelet Learning Rate	0.001
Learning Rate	0.01
L1 Regularization Factor	0.01
L2 Regularization Factor	0.1
# Epochs	15
# Wavelet Kernels	4
Wavelet Kernels Frequency Range	[8, 30]
# Temporal Kernels	4
# CSP subspace vectors (m)	2
Loss Function Ratio	0.3
Feature Reduction Network Layers	[16, 8, 4]

5. LDA

In this step, a Linear Discriminant Analysis (LDA) was implemented for the final classification. By receiving the weights of the four neurons of the last layer of the FRN, having the class labels, the LDA solves a generalized eigenvalue problem (GEP) to find a transform that reduces the dimension of the LDA inputs to one:

$$X_L^{b \times 4}, Label_{input} \xrightarrow{\text{solve GEP}} W_L^{4 \times 1} \quad (20)$$

The transform is then applied to the LDA input to create a one-dimensional vector:

$$Y^b = W_L^T \times X_L^T \quad (21)$$

Where Y^b is the LDA feature vector.

To predict unlabeled data in the form of the FRN output and a vector with size four ($x_i \in \mathbb{R}^4$) with the LDA, the distance to the mean of each class's extracted feature vector (Y_{class0} and Y_{class1} extracted from Y^b) will be calculated, and the class with the minimum distance will be chosen as the predicted label.

The second loss function, named LDALoss is defined as below to minimize the variance of each class's LDA feature vector (Y_{class0} and Y_{class1}) and maximize the distance between their means:

$$LDALoss(Y^b) = \frac{[var(Y_{class0}) + var(Y_{class1})]}{[mean(Y_{class0}) - mean(Y_{class1})]^2} \quad (22)$$

This loss function is used for updating the weights of the feature-reduction network.

The cumulative loss function, which is used to update the WKCNN and the TCNN weights is the weighted sum of the two loss functions (15) and (22):

$$totLoss = lossRatio \times CSPLoss + (1 - lossRatio) \times MVLoss \quad (23)$$

Where $lossRatio = 0.3$ in the final proposed framework. As stated before, the effect of $CSPLoss$ is to reduce overfitting. Therefore, the $lossRatio$ acts to create a balance between overfitting and underfitting, and to resolve the bias-variance trade-off.

In essence, CCSPNet integrates five modules with multiple functionalities into a consistent trainable framework that processes input signals to achieve the best classification performance. Algorithm 1 outlines the described classification process.

C. Implementation and Evaluation

The full list of selected hyperparameters for the framework in both subject-dependent and subject-independent approaches are listed in Table II. The framework was implemented using PyTorch [59]. Specifically, the CSP and LDA were implemented from scratch using PyTorch tensors to make their parameters trainable and make them compatible with gradient calculation and backpropagation. Adam optimization algorithm [55] was used for training the framework.

To evaluate the framework's performance and further compare its results in both SD and SI approaches with other frameworks', training and test sets are created as described below:

For the subject-dependent approach, 300 trials belonging to the training and test parts of session one and the training part of session two are used for training. The test data of session 2 is used as the test set.

To evaluate the classification performance of the subject-independent approach, the leave-one-subject-out cross-validation (LOSO-CV) method was utilized. In LOSO-CV, a separate model is trained for every 54 subjects, by using the session two test data of the other 53 subjects (5300 trials in total (Other trials are discarded in the SI approach.)) as the training set, and the same test set as the SD paradigm. The final subject-independent accuracy is calculated by averaging over all 54 LOSO-CV SI accuracies.

V. RESULTS

In Table IV, the classification accuracies of all 54 subjects with different methods and approaches are presented (all results are obtained on the same test set.). The best method performance for each subject is indicated by bold numbers in this table. In Table III, the summary of classification performances of all SD and SI methods trained on the dataset are presented. The CSP, FBCSP [60], CSSP [61], BSSFO [62], results are used by the recorders of the dataset to evaluate their online classifiers performance [21]. Pooled CSP [41], Fused model [63], and MR FBCSP [41] results are obtained by Kwon *et al.* [44] to compare the performance of their proposed method with other subject-independent methods. To evaluate the

performance of EEGNet in the subject-dependent approach, the preprocessed EEG data were given to this framework as the model input. The hyperparameters of EEGNet were set to default [26]. To better illustrate the performance of the

CCSPNet framework, six scatter plots are drawn in Fig 4. The first five plots compare the subject-dependent results of CCSPNet with other SD methods. The final plot shows the accuracy of the SI approach versus the SD approach obtained by CCSPNet.

TABLE III. Summarized results and performance comparison between different subject-dependent and subject-independent methods and frameworks

Approach	Method	Mean Accuracy	Standard Deviation
Subject-dependent	CSP [21]	68.57	17.57
	CSSP [21]	69.68	18.53
	FBCSP [21]	70.59	18.56
	BSSFO [21]	71.02	18.83
	Kwon <i>et al.</i> [44]	71.32	15.88
	EEGNet [26]	65.31	18.72
	CCSPNet (Proposed)	73.55	17.72
Subject-independent	Pooled CSP [44]	65.65	16.11
	Fused model [44]	67.37	16.01
	MR FBCSP [44]	68.59	15.28
	Kwon <i>et al.</i> [44]	74.15	15.83
	CCSPNet (Proposed)	74.11	15.42

VI. DISCUSSION AND ANALYSIS

The proposed framework is a fusion of signal processing, traditional machine learning, and deep learning. The total number of parameters (including CSP and LDA parameters) is only 5036.

Our framework utilizes wavelet transforms and temporal convolutions to create more discriminative inputs for the CSP. Temporal convolution has also been utilized by Lawhern *et al.* in their EEGNet to learn frequency filters. The motivation behind adding the WKCNN behind this TCNN will be further discussed below.

By analyzing the subject-dependent results in Table IV for CSP-based methods, EEGNet, and the CCSPNet framework, we can see that using deep-learning-based dynamic filters and a novel CSP feature reduction method, our framework has been able to outperform the mentioned methods. The effectiveness of the combination of WKCNN and TCNN in our architecture is visualized in two figures.

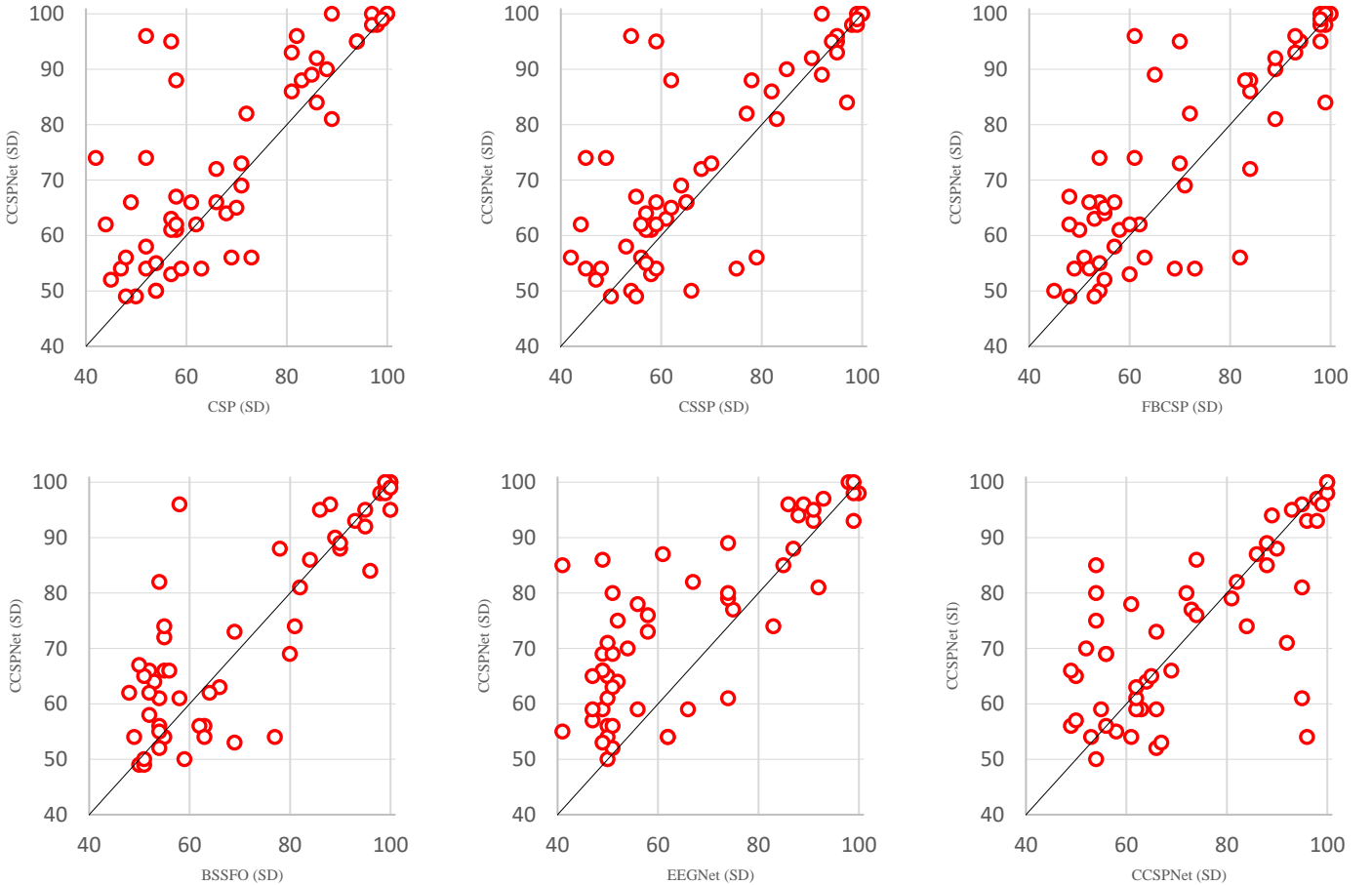


Fig 4. Scatter plots comparing the classification performance of the CCSPNet framework with other subject-dependent methods. In the first five plots, the horizontal axis presents the percentage accuracy of a SD method, and the vertical axis presents the percentage accuracy of the CCSPNet SD approach. The final plot compares the SD and SI accuracies obtained by the CCSPNet.

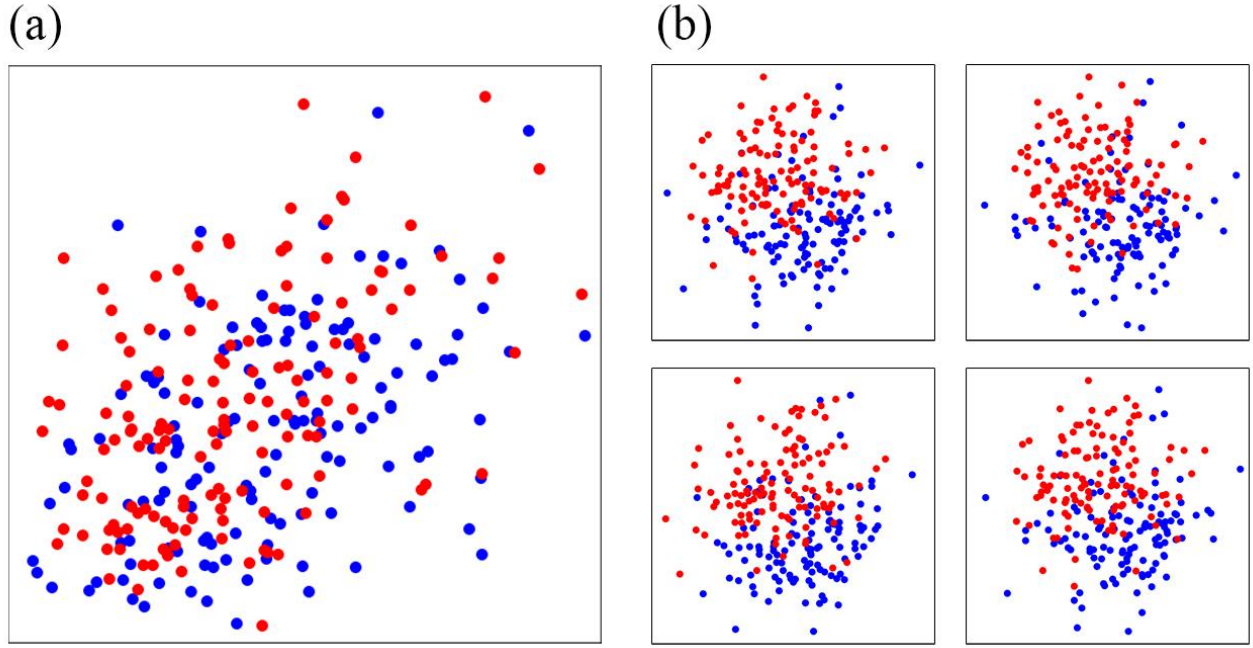


Fig 5. a) The raw CSP output of a subject with a poor performance using CSP-based methods. b) The CSP outputs of the same subject using the CCSPNet proposed framework. The red and blue points represent the two distinct classes feature vectors. The CSP performance can be gaged by its ability to separately cluster each class feature points and separate them from the opposite class's.

Fig. 5-a shows the raw CSP output of a subject with a poor performance using the CSP-based SD method. Fig. 5-b shows the CSP outputs (for each TCNN filter output) of the same subject using the CCSPNet framework. Since the CSP feature vector size is four, the first and the last features are extracted to represent the feature vector in a 2-D plot. The red and blue points indicate the feature points of each class. The performance of the CSP can be gaged by its ability to cluster the features of each class together and separate them from the opposite class's. From this figure, it is evident that the dynamic

WKCNN-TCNN filters have been successful in detecting frequencies that are more distinguishable by the CSP. This DL-based optimized filtering may be the main reason behind the fact that, as shown in Fig. 4, the proposed framework outperforms the CSP-based methods.

Fig. 6-a shows three time-frequency plots (using short-time Fourier transform (STFT)) for a specific subject and EEG channel (electrode). These contours are plotted before any preprocessing, after WKCNN, and after the WKCNN-TCNN filters. By analyzing these plots, the following can be observed:

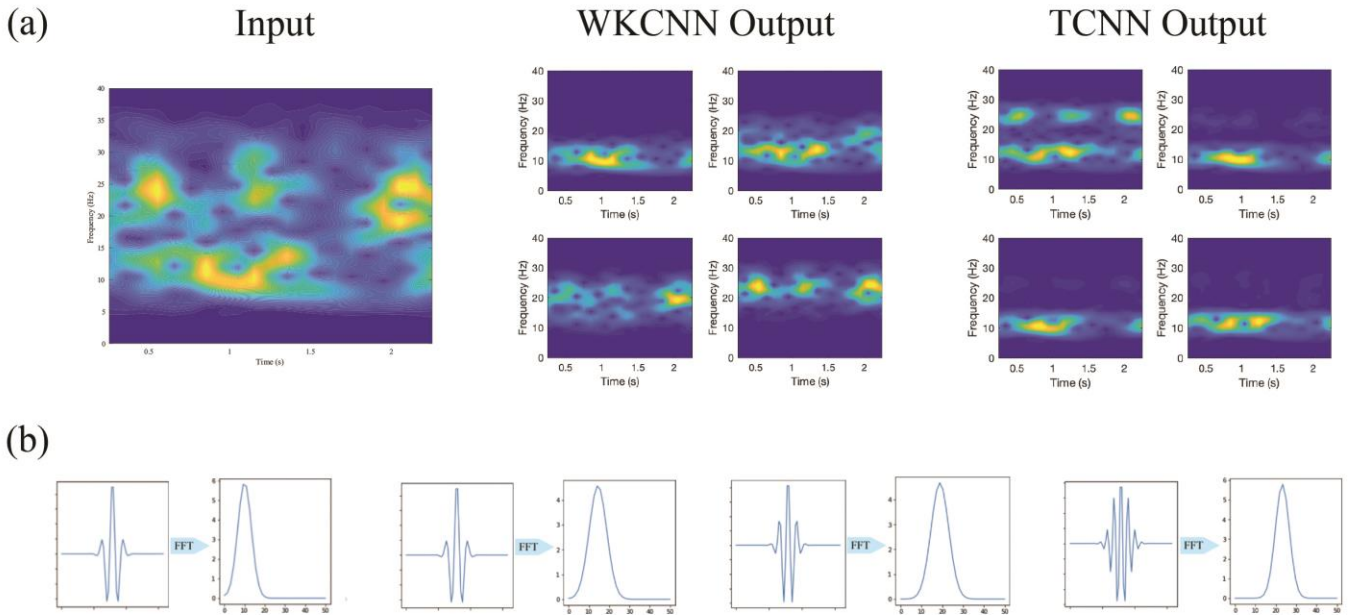


Fig 6. a) Time-frequency (STFT) plots for a specific subject and EEG channel (electrode). b) Four wavelet kernels with their corresponding frequency plot.

Normal convolutional kernels are not represented by a specific mathematical function. They are more flexible and can select various frequencies to filter the data. On the other hand, wavelet kernels are constructed using an analytical expression. They have a shape corresponding to this expression. Wavelets have a strict filtering policy and filter the data to a specific frequency range. This is illustrated in Fig 6-b by plotting four wavelets and their frequency plots using fast Fourier transform (FFT). The trade-off between filtering rigidness and flexibility in the WKCNN-TCNN combination, is exploited in the proposed architecture. As illustrated in Fig 6-a, First, the WKCNN discovers meaningful features in specific frequency ranges. Afterward, the TCNN combines the spectral features detected by different wavelet frequencies to create more generalizable features. These features are especially important in the subject-independent approach. We hypothesize that the TCNN may be able to combine the specific WKCNN features extracted from different subjects to create generalizable features for all subjects, which in turn can help improve the performance of subjects with low accuracy in the subject-dependent approach who may not possess inherent brain patterns that could help them achieve a better performance in the SD approach.

By comparing the SI and SD results of CCSPNet from Table IV and Fig 4, we can see that the subject-independent model has increased the classification accuracy many of the subjects with poor and mediocre performance while decreasing some excellent subjects' accuracies. This phenomenon can be explained by the hypothesis mentioned in the previous paragraph that the subject-independent deep learning framework utilizes the large number of available trials and the aforementioned WKNN-TCNN technique to extract generalizable features from all subjects' brain signals that may help improve the performance of subjects with low or average SD performance without inherent brain signal patterns. On the other hand, as hypothesized by Kwon *et al.* [44], subjects with excellent subject-dependent accuracy may have their own specific and inherent EEG signal features that are responsible for their excellent SD performance. Therefore, applying a model with generalizable features to them may result in a performance deterioration. This reduction in excellent subjects' classification accuracy is not a concern, because in a real application, when we detect that a person has an excellent BCI performance, we can, for example, change the mode of the BCI classifier to subject-dependent and use the subject's own EEG signals to fine-tune the SD classifier. Conversely, improving the poor and average-performing subjects' accuracy is a great achievement for the SI framework, because due to the lack of inherent brain patterns, this enhancement is much harder than achieving high accuracies with excellent and experienced BCI users.

A result of this enhancement, in this case for average-performing subjects, is that the number of BCI-illiterate users, based on the illiteracy metric defined by Lee *et al.* [21], is reduced from 28 to 24 by the CCSPNet subject-independent framework. Although the proposed framework has been partially successful in this low and average performance enhancement by using dynamic filtering and taking advantage of generalizable features, there is still room for improving the

performance of these types of subjects by utilizing other novel techniques in the future.

VII. CONCLUSION

In this research, we have proposed a compact subject-independent framework for the classification of motor imagery brain-computer interface tasks named CCSPNet. This hybrid framework takes advantage of a wavelet kernel convolutional neural network, a temporal convolutional neural network, CSP, and a dense neural network to outperform and compete with other subject-dependent and subject-independent methods on a large-scale motor imagery database. The compactness of this framework makes it a suitable candidate for low-power BCI applications.

The compactness and the high SD and SI accuracy achieved together by our framework is to this date extremely scarce in the motor imagery, and generally in the BCI literature. However, as we will move further into the future and the fourth industrial revolution continues to unfold, the use of similar compact frameworks with possibly more novel approaches and architectures, in real-world BCI and IoT, will become more significant.

TABLE IV. Classification results (percentage) for all subjects and different methods and frameworks

Method Subject	CSP (SD) [21]	CSSP (SD) [21]	FBCSP (SD) [21]	BSSFO (SD) [21]	EEGNet (SD) [26]	CCSPNet (proposed) (SD)	CCSPNet (proposed) (SI)
1	83	78	84	90	85	88	85
2	86	97	99	96	83	84	74
3	94	95	94	95	89	95	96
4	57	61	53	66	56	63	59
5	81	82	84	84	61	86	87
6	88	85	89	89	87	90	88
7	71	64	71	80	49	69	66
8	66	68	84	55	51	72	80
9	71	70	70	69	75	73	77
10	61	65	54	52	66	66	59
11	50	50	48	50	50	49	56
12	58	58	50	54	50	61	54
13	54	54	54	59	50	50	65
14	48	55	53	51	49	49	66
15	57	58	60	69	62	53	54
16	69	56	63	63	49	56	69
17	42	45	54	55	58	74	76
18	82	95	93	88	91	96	93
19	89	83	89	82	74	81	79
20	73	79	82	62	51	56	69
21	100	100	100	100	100	100	98
22	85	92	65	90	88	89	94
23	68	57	55	53	52	64	64
24	54	66	45	51	47	50	57
25	57	59	70	86	74	95	61
26	44	44	48	48	49	62	59
27	70	62	55	51	47	65	65
28	97	99	98	99	98	100	100
29	98	98	99	98	99	98	93
30	66	65	57	55	58	66	73
31	57	57	58	58	56	61	78
32	97	99	98	99	93	98	97
33	89	92	100	100	99	100	98
34	47	45	49	55	50	54	50
35	52	54	61	58	62	96	54
36	94	94	98	100	92	95	81
37	81	95	93	93	91	93	95
38	52	53	57	52	41	58	55
39	52	49	61	81	49	74	86
40	58	56	62	64	50	62	61
41	48	42	51	54	51	56	56
42	63	75	73	77	52	54	75
43	86	90	89	95	50	92	71
44	100	100	99	99	99	100	100
45	99	99	98	100	86	99	96
46	58	62	83	78	74	88	89
47	59	59	69	63	41	54	85
48	49	59	52	56	51	66	52
49	62	59	60	52	51	62	63
50	58	55	48	50	49	67	53
51	52	48	52	49	74	54	80
52	72	77	72	54	67	82	82
53	54	57	54	54	47	55	59
54	45	47	55	54	54	52	70
Mean	68.57	69.69	70.59	71.02	65.31	73.55	74.11
Standard Deviation	17.57	18.53	18.56	18.83	18.72	17.72	15.42
Median	64.5	63	64	63.5	57	67	73.5
Range	58	58	55	52	59	49	50
# BCI illiterate subjects	31	31	32	29	34	28	24

REFERENCES

- [1] E. C. Leuthardt, G. Schalk, J. R. Wolpaw, J. G. Ojemann, and D. W. Moran, "A brain-computer interface using electrocorticographic signals in humans," *J. Neural Eng.*, vol. 1, no. 2, pp. 63–71, 2004.
- [2] G. Schalk, D. J. Mcfarland, T. Hinterberger, N. Birbaumer, J. R. Wolpaw, and A. B. I. B. C. I. Technology, "BCI2000: A General-Purpose Brain-Computer Interface (BCI) System," vol. 51, no. 6, pp. 1034–1043, 2004.
- [3] "3.pdf," <https://www.gtec.at/product/>.
- [4] G. Pfurtscheller and C. Neuper, "Motor imagery direct communication," *Proc. IEEE*, vol. 89, no. 7, pp. 1123–1134, 2001.
- [5] N. Lu, T. Li, X. Ren, and H. Miao, "A Deep Learning Scheme for Motor Imagery Classification based on Restricted Boltzmann Machines," *IEEE Trans. Neural Syst. Rehabil. Eng.*, vol. 25, no. 6, pp. 566–576, 2017.
- [6] J. Höhne, M. Schreuder, B. Blankertz, and M. Tangermann, "A novel 9-class auditory ERP paradigm driving a predictive text entry system," *Front. Neurosci.*, vol. 5, no. AUG, pp. 1–10, 2011.
- [7] C. Wu, K. Lin, W. Wu, and X. Gao, "A novel algorithm for learning sparse spatio-spectral patterns for event-related potentials," *IEEE Trans. Neural Networks Learn. Syst.*, vol. 28, no. 4, pp. 862–872, 2017.
- [8] O. Friman, I. Volosyak, and A. Graser, "Multiple Channel Detection of Steady-State Visual Evoked Potentials for Brain-Computer Interfaces," *IEEE Trans. Biomed. Eng.*, vol. 54, no. 4, pp. 742–750, Apr. 2007.
- [9] J. Decety, "Brain Structures Participating in Mental," *Acta Psychol. (Amst.)*, vol. 73, pp. 13–34, 1990.
- [10] C. Neuper, R. Scherer, M. Reiner, and G. Pfurtscheller, "Imagery of motor actions: Differential effects of kinesthetic and visual-motor mode of imagery in single-trial EEG," *Cogn. Brain Res.*, vol. 25, no. 3, pp. 668–677, 2005.
- [11] D. Bright, A. Nair, D. Salvekar, and S. Bhisikar, "EEG-based brain controlled prosthetic arm," *Conf. Adv. Signal Process. CASP 2016*, pp. 479–483, 2016.
- [12] S. Jacob, V. G. Menon, F. Al-Turjman, P. G. Vinoj, and L. Mostarda, "Artificial Muscle Intelligence System with Deep Learning for Post-Stroke Assistance and Rehabilitation," *IEEE Access*, vol. 7, pp. 133463–133473, 2019.
- [13] M. Wang, R. Li, R. Zhang, G. Li, and D. Zhang, "A Wearable SSVEP-Based BCI System for Quadcopter Control Using Head-Mounted Device," *IEEE Access*, vol. 6, no. c, pp. 26789–26798, 2018.
- [14] J. Li, J. Liang, Q. Zhao, J. Li, K. Hong, and L. Zhang, "Design of assistive wheelchair system directly steered by human thoughts," *Int. J. Neural Syst.*, vol. 23, no. 3, pp. 1–12, 2013.
- [15] I. Lee and K. Lee, "The Internet of Things (IoT): Applications, investments, and challenges for enterprises," *Bus. Horiz.*, vol. 58, no. 4, pp. 431–440, 2015.
- [16] W. Shi, J. Cao, Q. Zhang, Y. Li, and L. Xu, "Edge Computing: Vision and Challenges," *IEEE Internet Things J.*, vol. 3, no. 5, pp. 637–646, 2016.
- [17] W. Shi and S. Dustdar, "CLOUD COVER WHY DO WE NEED EDGE COMPUTING? The Promise of Edge Computing," no. 0018, 2016.
- [18] <https://www.emotiv.com/epoc-x/>.
- [19] <https://shop.openbci.com/collections/frontpage/headw> are.
- [20] S. Rajesh, V. Paul, V. G. Menon, S. Jacob, and P. Vinod, "Secure Brain-to-Brain Communication With Edge Computing for Assisting Post-Stroke Paralyzed Patients," *IEEE Internet Things J.*, vol. 7, no. 4, pp. 2531–2538, 2020.
- [21] M. Lee *et al.*, "EEG Dataset and OpenBMI Toolbox for Three BCI Paradigms: An Investigation into BCI Illiteracy," pp. 1–15, 2017.
- [22] L. Qin, L. Ding, and B. He, "Motor imagery classification by means of source analysis for brain-computer interface applications," *J. Neural Eng.*, vol. 1, no. 3, pp. 135–141, 2004.
- [23] L. Qin, B. Kamousi, Z. M. Liu, L. Ding, and B. He, "Classification of motor imagery tasks by means of time-frequency-spatial analysis for Brain-Computer Interface applications," *2nd Int. IEEE EMBS Conf. Neural Eng.*, vol. 2005, no. 2, pp. 374–376, 2005.
- [24] R. Iru *et al.*, "Common Spatial Pattern Method for Channel Selection in Motor Imagery Based BCI," pp. 5392–5395, 2005.
- [25] E. Dong, C. Li, L. Li, S. Du, A. N. Belkacem, and C. Chen, "Classification of multi-class motor imagery with a novel hierarchical SVM algorithm for brain-computer interfaces," *Med. Biol. Eng. Comput.*, vol. 55, no. 10, pp. 1809–1818, 2017.
- [26] D. verma Atul, "EEGNet: A Compact Convolutional NN for EEG-based BCI," *Certain distance degree based Topol. indices Zeolite LTA Fram.*, no. December 2016, pp. 11–14, 2018.
- [27] W. Huang, Y. Xue, L. Hu, and H. Liuli, "S-EEGNet: Electroencephalogram Signal Classification Based on a Separable Convolution Neural Network with Bilinear Interpolation," *IEEE Access*, vol. 8, pp. 131636–131646, 2020.
- [28] X. Wang, M. Hersche, B. Tomekce, B. Kaya, M. Magno, and L. Benini, "An Accurate EEGNet-based Motor-Imagery Brain-Computer Interface for Low-Power Edge Computing," *IEEE Med. Meas. Appl. MeMeA 2020 - Conf. Proc.*, 2020.
- [29] T. Schneider, X. Wang, M. Hersche, L. Cavigelli, and L. Benini, "Q-EEGNet: An energy-efficient 8-bit quantized parallel EEGNet implementation for edge motor-imagery brain-machine interfaces," *arXiv*, 2020.
- [30] M. X. Cohen, "A better way to define and describe Morlet wavelets for time-frequency analysis," *Neuroimage*, vol. 199, no. September 2018, pp. 81–86, 2019.
- [31] Z. Zhang *et al.*, "A Novel Deep Learning Approach with Data Augmentation to Classify Motor Imagery Signals," *IEEE Access*, vol. 7, pp. 15945–15954, 2019.
- [32] T. H. Shovon, Z. Al Nazi, S. Dash, and M. F. Hossain, "Classification of motor imagery EEG signals with

- multi-input convolutional neural network by augmenting STFT,” *2019 5th Int. Conf. Adv. Electr. Eng. ICAEE 2019*, no. August, pp. 398–403, 2019.
- [33] Y. R. Tabar and U. Halici, “A novel deep learning approach for classification of EEG motor imagery signals,” *J. Neural Eng.*, vol. 14, no. 1, p. 16003, 2017.
- [34] J. Dinarès-Ferran, R. Ortner, C. Guger, and J. Solé-Casals, “A new method to generate artificial frames using the Empirical Mode Decomposition for an EEG-based motor imagery BCI,” *Front. Neurosci.*, vol. 12.
- [35] I. J. Goodfellow *et al.*, “Generative adversarial nets,” *Adv. Neural Inf. Process. Syst.*, vol. 3, no. January, pp. 2672–2680, 2014.
- [36] F. Fahimi, S. Dosen, K. K. Ang, N. Mrachacz-Kersting, and C. Guan, “Generative Adversarial Networks-Based Data Augmentation for Brain-Computer Interface,” *IEEE Trans. Neural Networks Learn. Syst.*, pp. 1–13.
- [37] Q. Zhang and Y. Liu, “Improving brain computer interface performance by data augmentation with conditional Deep Convolutional Generative Adversarial Networks.”
- [38] F. Fahimi, Z. Zhang, W. B. Goh, T. S. Lee, K. K. Ang, and C. Guan, “Inter-subject transfer learning with an end-to-end deep convolutional neural network for EEG-based BCI,” *J. Neural Eng.*, vol. 16, no. 2, 2019.
- [39] S. Sakhavi and C. Guan, “Convolutional neural network-based transfer learning and knowledge distillation using multi-subject data in motor imagery BCI,” *Int. IEEE/EMBS Conf. Neural Eng. NER*, pp. 588–591, 2017.
- [40] V. Jayaram, M. Alamgir, Y. Altun, and M. Grosse-wentrup, “Transfer Learning in Brain-Computer Interfaces,” no. January, pp. 20–31, 2016.
- [41] F. Lotte, C. Guan, and K. K. Ang, “Comparison of designs towards a subject-independent brain-computer interface based on motor imagery,” *Proc. 31st Annu. Int. Conf. IEEE Eng. Med. Biol. Soc. Eng. Futur. Biomed. EMBC 2009*, pp. 4543–4546, 2009.
- [42] B. Reuderink, J. Farquhar, M. Poel, and A. Nijholt, “A subject-independent brain-computer interface based on smoothed, second-order baselining,” *Proc. Annu. Int. Conf. IEEE Eng. Med. Biol. Soc. EMBS*, pp. 4600–4604, 2011.
- [43] Y. LeCun, Y. Bengio, and G. Hinton, “Deep learning,” *Nature*, vol. 521, no. 7553, pp. 436–444, May 2015.
- [44] O. Y. Kwon, M. H. Lee, C. Guan, and S. W. Lee, “Subject-Independent Brain-Computer Interfaces Based on Deep Convolutional Neural Networks,” *IEEE Trans. Neural Networks Learn. Syst.*, vol. 31, no. 10, pp. 3839–3852, 2020.
- [45] <http://gigadb.org/dataset/view/id/100542>.
- [46] C. Neuper, M. Wörtz, and G. Pfurtscheller, “Chapter 14 ERD/ERS patterns reflecting sensorimotor activation and deactivation,” *Prog. Brain Res.*, vol. 159, pp. 211–222, 2006.
- [47] H. J. LANDAU, “Sampling, Data Transmission, and the Nyquist Rate,” *Proc. IEEE*, vol. 55, no. 10, pp. 1701–1706, 1967.
- [48] K. J. Miller, G. Schalk, E. E. Fetz, M. den Nijs, J. G. Ojemann, and R. P. N. Rao, “Cortical activity during motor execution, motor imagery, and imagery-based online feedback,” *Proc. Natl. Acad. Sci.*, vol. 107, no. 9, pp. 4430–4435, Mar. 2010.
- [49] L. He, Y. Hu, Y. Li, and D. Li, “Channel selection by Rayleigh coefficient maximization based genetic algorithm for classifying single-trial motor imagery EEG,” *Neurocomputing*, vol. 121, pp. 423–433, 2013.
- [50] K. Tavakolian, A. M. Nasrabadi, and S. Rezaei, “Selecting better EEG channels for classification of mental tasks,” *Proc. - IEEE Int. Symp. Circuits Syst.*, vol. 3, 2004.
- [51] P. Ofner, A. Schwarz, J. Pereira, D. Wyss, R. Wildburger, and G. R. Müller-Putz, “Attempted Arm and Hand Movements can be Decoded from Low-Frequency EEG from Persons with Spinal Cord Injury,” *Sci. Rep.*, vol. 9, no. 1, pp. 1–15, 2019.
- [52] P. Wang, A. Jiang, X. Liu, J. Shang, and L. Zhang, “LSTM-based EEG classification in motor imagery tasks,” *IEEE Trans. Neural Syst. Rehabil. Eng.*, vol. 26, no. 11, pp. 2086–2095, 2018.
- [53] T. Li, S. Member, Z. Zhao, C. Sun, and L. Cheng, “WaveletKernelNet: An Interpretable Deep Neural Network for Industrial Intelligent Diagnosis Tianfu.”
- [54] S. Sakhavi, C. Guan, and S. Yan, “Learning Temporal Information for Brain-Computer Interface Using Convolutional Neural Networks,” *IEEE Trans. Neural Networks Learn. Syst.*, vol. 29, no. 11, pp. 5619–5629, Nov.
- [55] D. P. Kingma and J. L. Ba, “Adam: A method for stochastic optimization,” *3rd Int. Conf. Learn. Represent. ICLR 2015 - Conf. Track Proc.*, pp. 1–15, 2015.
- [56] <https://pytorch.org/docs/stable/generated/torch.nn.BCELoss.html>.
- [57] H. Yu and J. Yang, “A direct LDA algorithm for high-dimensional data — with application to face recognition,” *Pattern Recognit.*, vol. 34, no. 10, pp. 2067–2070, 2001.
- [58] X. S. Zhuang and D. Q. Dai, “Improved discriminate analysis for high-dimensional data and its application to face recognition,” *Pattern Recognit.*, vol. 40, no. 5, pp. 1570–1578, 2007.
- [59] A. Paszke *et al.*, “Automatic differentiation in PyTorch,” no. Nips, pp. 1–4, 2017.
- [60] K. K. Ang, Z. Y. Chin, H. Zhang, and C. Guan, “Filter Bank Common Spatial Pattern (FBCSP) in brain-computer interface,” *Proc. Int. Jt. Conf. Neural Networks*, pp. 2390–2397, 2008.
- [61] S. Lemm, B. Blankertz, G. Curio, and K. R. Müller, “Spatio-spectral filters for improving the classification of single trial EEG,” *IEEE Trans. Biomed. Eng.*, vol. 52, no. 9, pp. 1541–1548, 2005.
- [62] H. Il Suk and S. W. Lee, “A novel bayesian framework for discriminative feature extraction in brain-computer interfaces,” *IEEE Trans. Pattern Anal. Mach. Intell.*, vol. 35, no. 2, pp. 286–299, 2013.
- [63] A. M. Ray *et al.*, “A subject-independent pattern-based brain-computer interface,” *Front. Behav. Neurosci.*, vol. 9, no. OCTOBER, pp. 1–15, 2015.



Mahbod Nouri received the B.S. degree in mechanical engineering from University of Tehran, Iran, in 2020.

In summer 2020, he was an intern and research assistant with the Artificial Intelligence in Mechanical Engineering (AIME) Lab, University of Tehran. He is currently a research assistant with the Advanced Robotics and Intelligent

Systems Lab, School of ECE, University of Tehran, Iran. His current research interests include machine learning, brain-computer interfaces, deep learning, signal processing, and computer vision.

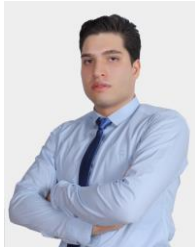
full Professor there. He is also a scientific advisor at the National Brain Mapping Laboratory, located at University of Tehran, Iran. His current research interests include brain-computer interfaces, biomedical signal processing, machine learning, deep learning, nonlinear time series analysis, and computational neuroscience.

Dr. Nasrabadi is a board member of the Iranian Society for Biomedical Engineering and has served on the scientific committees of several national conferences and review boards of five scientific journals.



Faraz Moradi received the B.S. degree in biomedical engineering from Islamic Azad University, Science and Research Branch, Tehran, Iran, in 2020.

His current research interests include Brain-Computer Interfaces, Neuroscience, Signal Processing, Machine Learning, and Deep Learning.



Hafez Ghaemi received the B.S. degree in mechanical engineering with a minor in computer engineering from University of Tehran, Iran, in 2020. He is currently perusing the M.S. degree in Data Science and Engineering at Polytechnic University of Turin, Italy, and the ASP joint program between Polytechnic Universities of Milan and

Turin, Italy.

From 2019 to 2020, he was a research assistant with the Artificial Intelligence in Mechanical Engineering (AIME) Lab, University of Tehran. His current research interests include machine learning, reinforcement learning, brain-computer interfaces, deep learning, and signal processing.

Mr. Ghaemi is a recipient of the TOPoliTO scholarship.



Ali Motie Nasrabadi received the B.S. degree in Electronic Engineering in 1994 and the M.S. and Ph.D. degrees in Biomedical Engineering in 1999 and 2004 respectively, from Amirkabir University of Technology, Tehran, Iran.

In 2004, he joined the biomedical engineering department, Faculty of Engineering, Shahed University. From

2004 to 2011 he was an Assistant Professor, from 2011 to 2017 he was an Associate Professor and since 2017, he has been a